# Scenario for the 0.7-conductance anomaly in quantum point contacts

Anton A. Starikov,[1,2] Irina I. Yakimenko,[1] and Karl-Fredrik Berggren[1]
[1]*Department of Physics and Measurement Technology, Linköping University, S-581 83 Linköping, Sweden*
[2]*Kirensky Institute of Physics, 660036 Krasnoyarsk, Russia*
(Received 26 December 2002; published 23 June 2003)

Effects of spontaneous spin polarization in quantum point contacts (QPC's) are investigated for a realistic semiconductor device structure using the Kohn-Sham local spin-density formalism. At maximal polarization in the contact area, there is a bifurcation into ground-state and metastable solutions. The conduction associated with the metastability is lower than for the normal state. With increasing temperature, the conductance should therefore show an anomalous behavior as observed. For the present device we do not recover resonance or quasibound states.

DOI: 10.1103/PhysRevB.67.235319 PACS number(s): 73.61.−r, 71.15.Mb, 71.70.Gm

## I. INTRODUCTION

The ability to confine electrons spatially in a controlled way in layered semiconductor structures has led to the observation of remarkable properties of such structures. A celebrated example is the quantized conductance $G=2e^2n/h$, $n=1,2,3,\ldots$. in quantum point contacts (QPC's).[1,2] These ''normal'' conductance steps are now well understood in terms of noninteracting ballistic electrons. However, there is also an anomalous narrow plateau at noninteger values of $n$, the so-called ''0.7 anomaly,'' first studied in detail in Ref. 3. Since then this phenomenon has attracted increasing attention with many attempts to explain its origin, its peculiar temperature dependence, and response to magnetic field and source and drain bias, collectively referred to as the ''zero bias anomaly.'' Recent summaries and highlights are found, for example, in Refs. 4–7 and references therein.

Already, Thomas *et al.*[3] have pointed out the importance of spin. Consequently, spontaneous local spin polarization induced by electron interactions is thought to be an important mechanism underpinning the anomaly.[7,8] There are general difficulties, however, in explaining the observed anomalous temperature dependence in short wires using a simple static spin polarization model. Measurements suggest a Kondo-like mechanism[9,10] and models have been formulated in this spirit.[11,12] Of course, also a Kondo-related mechanism requires that there are localized moments related to the QPC. In the traditional Kondo picture these moments are, however, associated with bound states. It is not immediately clear how an open system such as a QPC may acquire bound states. Meir *et al.*[11] have circumvented this problem by assuming that there is a subset of scattering states that are resonant or quasibound states and therefore effectively act as the bound states. On this basis, an Anderson-Hamiltonian may be formulated and a Kondo-like conductance is obtained. Other recent propositions rely on a strictly one-dimensional Luttinger model.[13] In this case one finds a singlet ground state as $T\rightarrow 0$ and a spin-polarized state above a characteristic temperature $T_{wire}$. Although suggestive, it is not straightforward how to extend the model to a real semiconductor device structure.

In this paper, we will return to the model based on spontaneous spin-polarization using the Kohn-Sham local spin-density functional method (LSDA).[14] In previous work,[7] we simulated a realistic heterostructure device with a QPC connecting two relatively large dots. We also made rough estimates of the conductance using an approximate separable parabolic saddle potential. Artificial kinks in the conductance were, however, introduced in this way.

Here we will extend the simulations to a QPC in between two semi-infinite reservoirs (in practice, broad wires). In particular, we will study the nature of the QPC potential, local magnetization, and the conductance scattering states for a typical GaAs/AlGaAs device structure. For the present device, we do not recover resonance or quasibound states. On the other hand, we find that solutions to the LSDA equations bifurcate at a gate voltage at which the conductance anomaly is found. We suggest that these solutions, for ground state as well as for metastable states, have physical significance. The conductance of the metastable states is lower than for the normal state. As a consequence, one foresees an anomalous temperature dependence in the conductance as temperature is raised. This is evidently a different scenario for the QPC conductance anomaly.

Section II presents our model for the QPC, choice of exchange/correlation potentials, and selected computational aspects. Computational results for potentials, conduction, magnetization, and wave functions are discussed in Sec. III. Finally, Sec. IV contains a summary and concluding remarks.

## II. THEORETICAL MODEL AND METHOD OF CALCULATIONS

Quantum point contacts may be fabricated in modulation-doped heterostructure with patterned metallic top gate, see Fig. 1. A negative voltage applied to the gate relative to the substrate depletes the two-dimensional electron gas (2DEG) under the gated regions and leaves a conducting wire in the split-gate region.

The actual size of the quantum point contact and surrounding semi-infinite sections can be varied lithographically by changing the geometry of the gate as well as changing the applied voltage. The associated electrostatic confinement energy $e\tilde{V}_g$ that derives from the gate is obtained from the well-known expression:[15]

 

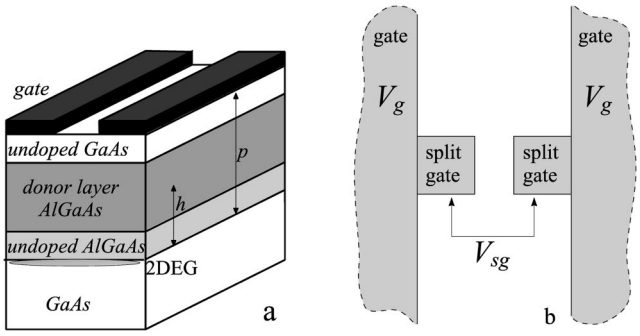


FIG. 1. (a) Schematic view of a modulation-doped GaAs/AlGaAs heterostructure with a patterned metallic gate; (b) Top view of the gate showing a narrow split-gate area that induces a QPC at the GaAs/AlGaAs interface. Upper and lower ungated areas indicate 2DEG reservoirs that serve as source and drain. To operate the device, two voltages $V_g$ and $V_{sg}$ are applied separately to the gated regions; $V_g$ and $V_{sg}$ regulate the effective width and electron density of the reservoirs and the QPC, respectively. An electric current flows through the QPC when a voltage difference $V_{sd}$ between the source and drain is set up.

$$e\tilde{V}_g(\mathbf{r},z)=\frac{1}{2\pi}\int d\mathbf{r}'\,eV_g(\mathbf{r}',0)\,\frac{|z|}{(z^2+|\mathbf{r}-\mathbf{r}'|^2)^{3/2}}, \quad (1)$$

where $V_g(\mathbf{r}',0)$ represents the potential on the different gated areas in Fig. 1(b), $z$ is the perpendicular distance between the gate and the 2DEG at the GaAs/AlGaAs interface, and $\mathbf{r}=(x,y)$ is the in-plane position. As indicated in the figure, we assume that there are four gated areas. The two semi-infinite gates [with constant $V_g(\mathbf{r}',0)=V_g$] give rise to two very wide straight channel areas that serve as electron reservoirs and source and drain when a current is passed through the system. The QPC itself is introduced by means of the two smaller gates and is controlled by $V_g(\mathbf{r}',0)=V_{sg}$.

To find the electronic configuration and related properties of the system we assume that the electron gas is strictly two dimensional and that the donor layer is fully ionized. The chemical potential $\mu$ is constant throughout the system and may be set equal to zero. We also assume the following boundary conditions: (i) the heterostructure is electrically neutral and the electric field vanishes at infinity; (ii) there is a Schottky barrier for electrons at the interface with the metallic gate ($eV_s=0.9$ eV); (iii) the wide source and drain regions are semi-infinite; (iv) at long distance from the QPC area the potential energy takes a constant value inside the two reservoirs.

Let us now consider the Kohn-Sham LSDA for our system. At zero temperature, the system is described by the effective one-electron equations for the two directions of spin $\sigma=\uparrow,\downarrow$:

$$-\frac{h^2}{2m^*}\nabla^2\Psi^\sigma(\mathbf{r})+[U_c(\mathbf{r})+U_{sc}^\sigma(\mathbf{r})]\Psi^\sigma(\mathbf{r})=E\Psi^\sigma(\mathbf{r}), \quad (2)$$

where $U_c$ is the confinement potential energy and $U_{sc}$ the self-consistent potential energy related to electron-electron interactions. The term

$$U_c(\mathbf{r})=eV_d+eV_s+e\tilde{V}_g(\mathbf{r}) \quad (3)$$

comprises contributions from gate (1), surface states $eV_s$, and the donor layer[15]

$$eV_d=-\frac{e^2}{\epsilon\epsilon_0}\rho_d d(c+d/2), \quad (4)$$

where $\rho_d=6\times10^{17}$ cm$^{-3}$ is the density of donors, and $c=24$ nm and $d=36$ nm are the thicknesses of the cap and the donor layer, respectively, and $\epsilon$ is the dielectric constant which we assume to be equal to 12.9 in this work. The self-consistent potential depends on electron densities and may be subdivided as

$$U_{sc}^\sigma(\mathbf{r})=U_e(\mathbf{r})+U_{ex}^\sigma(\mathbf{r})+U_{cr}^\sigma(\mathbf{r}), \quad (5)$$

where $U_e$ is the Hartree potential energy, $U_{cr}^\sigma$ is the correlation potential (for details see Ref. 16), and $U_{ex}^\sigma$ is the 2D electron exchange potential, which in the LSDA has the form

$$U_{ex}^\sigma(\mathbf{r})=-\frac{e^2}{\epsilon\epsilon_0\pi^{3/2}}[\rho^\sigma(\mathbf{r})]^{1/2}, \quad (6)$$

where $n^\sigma(\mathbf{r})$ is total density of electrons with spin $\sigma$. $U_{ex}^\sigma$ may be corrected for mirror charges but the effect turns out to be numerically small and may be neglected.

The Hartree potential energy $U_e(\mathbf{r})$ in Eq. (6) has the form

$$U_e(\mathbf{r})=\frac{1}{4\pi\epsilon\epsilon_0}\int d\mathbf{r}'\,\rho(\mathbf{r}')\left[\frac{1}{|\mathbf{r}-\mathbf{r}'|}-\frac{1}{\sqrt{|\mathbf{r}-\mathbf{r}'|^2+4z^2}}\right], \quad (7)$$

where $\rho(\mathbf{r})=\rho^\uparrow(\mathbf{r})+\rho^\downarrow(\mathbf{r})$ is the total density of electrons. The right-hand side of Eq. (7) contains the contribution from mirror charges related to the 2DEG.

Because we are interested in conduction, we construct the solutions as scattering states consisting of initial, reflected, and transmitted waves. Assume that the initial states enter from either the left ($L$) or from the right side ($R$) of the QPC. We write the first set of states as $\Psi_{Li}^\sigma(\mathbf{r},k_i)$, where $k_i$ is the wave number of an electron injected into the left reservoir in the $i$th spin subband. The total density for this kind of states with spin $\sigma$ is therefore

$$\rho_L^\sigma(\mathbf{r})=\frac{1}{2\pi}\sum_i\int_0^{k_{f_iL}^\sigma}|\Psi_{Li}^\sigma(\mathbf{r},k)|^2dk. \quad (8)$$

Index $i$ in the summation runs over all occupied subbands and the integration is over the corresponding wave numbers $k_i$ with the associated Fermi wave numbers $k_{f_iL}^\sigma$. In the same way, the density for states entering from the right is

$$\rho_R^\sigma(\mathbf{r})=\frac{1}{2\pi}\sum_i\int_0^{k_{f_iR}^\sigma}|\Psi_{Ri}^\sigma(\mathbf{r},-k)|^2dk. \quad (9)$$

The total 2D density of $\sigma$ electrons in the active area of the device is then

$$\rho^{\sigma}(\mathbf{r}) = \rho_L^{\sigma}(\mathbf{r}) + \rho_R^{\sigma}(\mathbf{r}). \tag{10}$$

The decomposition into left- and right-going waves means that also the total current $\mathbf{I}$ is decomposed in the same way as $\mathbf{I} = \mathbf{I}_R + \mathbf{I}_L$. By formulating the problem in this way it is clear how one may incorporate self-consistently the effects of a finite bias $V_{sd}$ and nonlinearity in the LSDA procedure. For our system, however, such computations easily become numerically exceedingly cumbersome.

To solve Eq. (2) numerically, a self-consistent iterative process was implemented in a rather standard fashion. As we will see, the numerics turns out to be delicate in many cases and for this reason we describe our procedure in more detail. For given values of $V_g$ and $V_{sg}$, we thus proceed in the following way.

(i) For a given potential $U_{sc}$, Eq. (2) is mapped onto a finite rectangular lattice located symmetrically around the QPC. Transparent boundary conditions[17] are used to match the corresponding solutions to the continuum scattering states in the two open semi-infinite reservoirs.

(ii) Assume that the bias voltage $V_{sd}$ is infinitesimally small. Hence numerical solutions are generated for all right- and left-going scattering states with energy $E$ less than a common Fermi energy $E_f$ (in our case $E_f = 0$). States for 60 equidistant values of $E$ were considered. Since the source and drain areas are wide, the number of subbands involved becomes large. Typically, 64 subband states have been included. At the Fermi energy, up to about 20 are propagating waves while the rest are evanescent states. At lowest energies just a few of them are propagating states.

(iii) The density of electrons with spin $\sigma$ is obtained from Eq. (10) and used to calculate a new potential $U_{sc}^{\sigma\,new}$ from Eq. (5).

(iv) The potential for the next iteration is obtained by the usual mixing procedure

$$(1-\alpha)U_{sc}^{\sigma\,new} + \alpha U_{sc}^{\sigma} \rightarrow U_{sc}^{\sigma},$$

which is inserted into Eq. (2). The mixing parameter $\alpha$ was used in the common way to increase the stability of the iteration process and was varied in a range of $[0.001; 0.02]$ depending on the convergence properties.

(v) As a criterion for convergence, we have used

$$\left\{ \sum_{\sigma=\uparrow,\downarrow} \sum_{j=1}^{N} [U_{sc}^{\sigma\,new}(j) - U_{sc}^{\sigma}(j)]^2 \right\}^{1/2} /(2N) \leqslant \gamma,$$

where $j$ denotes all the $N$ lattice points; typically $\gamma = 10^{-7}$ eV.

(vi) To initiate the spin-relaxed iterative procedure, we have either let the first choice for $U_{sc}^{\sigma}$ be a *random* potential or, when available, we have also chosen it from a previous calculation for a nearby value of the split-gate voltage $V_{sg}$.

The above iteration process was used to find electronic configurations, scattering states, potentials, and the conductance for different values of the split-gate voltage $V_{sg}$. For the cases reported here the voltage $V_g$ was set equal to 0.73 V. Lithographic dimensions of the patterned gate have been chosen as $100 \times 200$ nm$^2$ (width and length) for the middle channel in Fig. 1(b) and 500 nm for the width of the surrounding reservoirs. The size of the central numerical grid was typically $100 \times 200$.

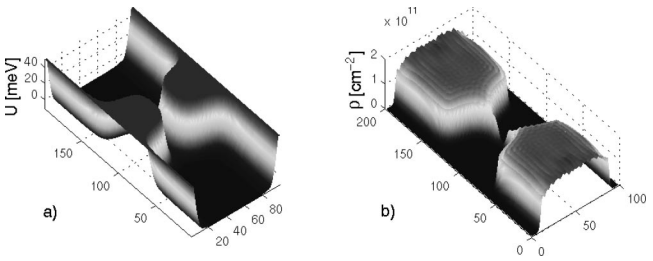


FIG. 2. (a) Typical total confinement potential $U = U_c + U_{sc}^{\sigma}$ for up-spin electrons at different grid points, and (b) electron density $\rho$ in the region of the quantum point contact at $V_{sg} = -0.723$ V.

Calculations were performed with (i) only the exchange term retained in the interaction potential, and with (ii) both exchange and correlation potentials included. The first case may be regarded as more exploratory. The iteration process appears more stable than in case (ii) and convergence is readily achieved because spin splitting gets exaggerated. About 300 iterations are needed for this case. We have therefore been able to follow the conductance behavior all the way into the third plateau. When also the correlation term $U_{cr}^{\sigma}$ is included about 500–600 iterations are required, which makes the computations quite tedious. Numerically, $U_{cr}^{\sigma}$ is much smaller than $U_{ex}^{\sigma}$. In spite of this it gives rise to delicate features that takes much care to uncover. Details are shown in the following section.

Finally, the conductance $G$ has been computed from the Landuaer-Büttiker formula $G = (2e^2/h)\mathrm{Tr}(TT^{+})$, where $T$ is a transmission matrix for the scattering solutions of Eq. (2) at the Fermi level. The expression for $G$ applies to the linear regime when $V_{sd} \rightarrow 0$, i.e., $\mathbf{I}_R \simeq -\mathbf{I}_L$ as assumed here.

## III. COMPUTATIONAL RESULTS

An overview of the total self-consistent confinement potential with exchange and correlation terms is shown in Fig. 2(a). In this resolution, the potential looks the same for the two spin directions. Figure 2(b) displays the total electron density $\rho$. As it should, $\rho$ is strongly reduced in the constriction. The behavior in the two reservoirs, where $\rho$ becomes practically constant as for a 2DEG, is also satisfactory. Numerical values are typical for real QPC devices.

The calculated conductance as a function of the applied gate voltage $V_{sg}$ is shown in Fig. 3. Case (a) represents the simplified model with exchange only, while (b) accounts for both exchange and correlation. Due to the numerical complexity of the problem, the conductance for model (b) is limited to the first plateau. Anomalies are evidently present in both curves, but at different values of $G$. The two lowest plateaus are well developed in case (a).

*Model with exchange only*. Let us first look at case (a) in more detail. The 0.5 plateau reconfirms previous results[18] although the present device modeling is much more realistic. The value of 0.5 tells that the QPC is locally fully spin polarized and that only one spin channel transmits. Compared

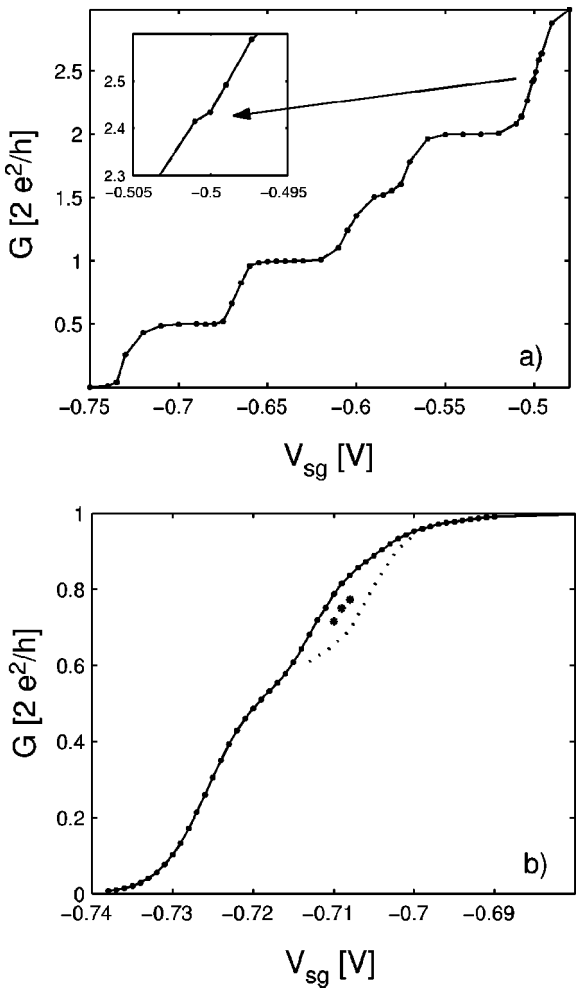


FIG. 3. Conductance versus gate voltage $V_{sg}$: (a) model with exchange potential only; (b) model with exchange and correlation potentials, ground-state solutions of Eq. (2) (solid line), and metastable states (dashed line and asterisks).

with experiments the anomalies are, however, too pronounced. Bare exchange thus appears to overdo spin splitting. In spite of this, the results support the idea that exchange interactions and local magnetization must be involved in a crucial way. Further support comes from the additional anomalies obtained for the second and third subbands in Fig. 3(a). These are in good qualitative agreement with experimental results[8,19,20] which show that the anomaly resurfaces in steps of $2e^2/h$ in higher subbands. As in observations, the anomaly gets much weaker in the second subband and is barely visible in the third. As to be expected from the discussion above, the conductance anomalies appear, however, at half values (actually 2.4 for the third subband due to increasing numerical inaccuracy at higher energies). At any rate, the results for the conductance anomalies in the higher subbands give further support to an exchange driven mechanism and spontaneous local spin polarization.

*Model with exchange and correlation*. If we now turn to case (b), there are obvious striking differences from (a) in spite of the relative smallness of the additional correlation term $U_{cr}^{\sigma}$. The reason is that the system is now just more

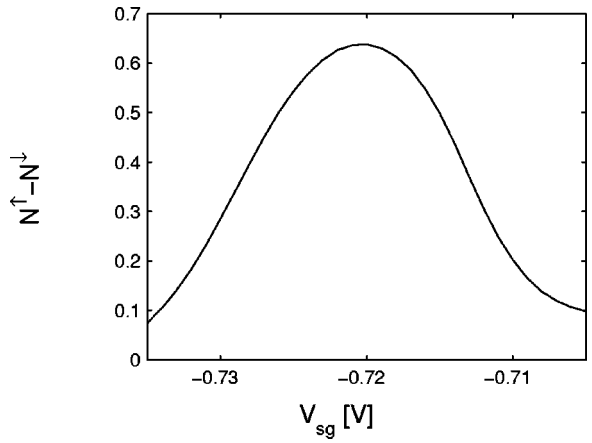


FIG. 4. Total number of spins $N^{\uparrow}-N^{\downarrow}$ in the QPC with correlation included. Numbers refer to the ground-state solutions in previous figure.

delicate. Whereas the self-consistent iteration scheme for case (a) shows good convergence and stability, case (b) reveals slower convergence and yields *more than one spin-polarized solution in a conspicuous range of voltages* $V_{sg}$. Some of the solutions are stable against small perturbations, while others turn out to be metastable. This was found out by a ''numerical shaking'' of the self-consistent solutions by momentarily adding a small random potential. If metastable, a solution then relaxes to a stable one as the perturbed system is brought to self-consistency by further iterations. The conductance obtained from the different kind of solutions is shown in Fig. 3(b). The solid line refers to the stable ground state. Metastable solutions, which are shown by the dotted line and by asterisks, are also important as discussed below. The solutions with asterisks are, however, much harder to find numerically and for this reason we are able to show only a limited set of points. These states are also more sensitive to the shake up procedure mentioned. A likely reason is that the corresponding energy minima are very shallow. It is remarkable that multisolutions appear at the apparent conduction anomaly at $\sim 0.6$ and persist in the region in which one observes an anomalous temperature behavior, i.e., there is a suppression of the measured conductance as the temperature is raised.

Having said that, there is an obvious scenario for the ''0.7-conduction'' anomaly. At zero temperature the conductance is determined by the ground-state solution [solid curve in Fig. 3(b)] *With increasing temperature also the metastable states become populated with increasing statistical weights. Consequently the conductance is gradually reduced with temperature, which would explain the observed anomalous behavior, at this stage in a qualitative way.*

*Polarization characteristics*. Irrespective of the two choices (a) and (b) for exchange and correlation potentials, the Kohn-Sham equation readily yields spin split solutions in relevant voltage regimes. An interesting question is how many spins are to be associated with the QPC. Figure 4 shows the total (integral) number of spins as a function of split-gate voltage,

$$N^{\uparrow}-N^{\downarrow}=\int d\mathbf{r}\Delta\rho_{spin}, \tag{11}$$

where $\Delta\rho_{spin}=\rho^{\uparrow}-\rho^{\downarrow}$ is the local spin density. A maximum value $\sim 0.6$ spins is obtained for $V_{sg}=0.717$ V, which is just the voltage at which one finds the first conduction anomaly in Fig. 3(b). The spin content is in good agreement with previous estimates[7,12] also based on the spin-polarized Kohn-Sham equations. Similar results are obtained for the half plateau in Fig. 3(a) and for the conductance structures in the higher subbands, although magnitudes become smaller with increasing subband index.

The spin polarization is mainly localized within the lithographic QPC region. It is accompanied by Friedel-like oscillations in the outer regions. There is a qualitative change in the local magnetization as one proceeds from pinch-off at $-0.74$ V in Fig. 3(b) towards the conductance anomaly at $-0.717$ V. At lowest voltages, there is a strong minimum right at the middle of the QPC. As the gate voltage is increased this dip gets more shallow and gradually disappears. Figures 5(a)–5(c) show the progression of the local spin density as the gate voltage $V_{sg}$ is varied in the very regime at which multisolutions appear and the magnetization maximizes. Just below the critical voltage $-0.717$ V there is thus a slight minimum in $\Delta\rho_{spin}$ [Fig. 5(a)], which evolves into a flat peak at the bifurcation point [Fig. 5(b)]. On further increase of $V_{sg}$, the maximum is smoothly rounded. The results in Fig. 5 refer to the Kohn-Sham ground-state solutions with the full exchange-correlation potential. Qualitatively, the same results are also found for the exchange model in Fig. 3(a). The pattern is repeated for the two higher subbands although the magnitudes are smaller.

Local spin densities and the presence of a deep minimum at certain voltages are also discussed in Refs. 7,12 for the ground-state subband. However, in the present case the minimum appears only at lowest electron concentrations. This difference might depend on different device geometries.

*Potential characteristics*. Figure 6 shows typical spin-polarized potentials along the middle transport direction. In the two cases shown, there is a clear difference in the height of the transmission barriers for the two spin directions, $\sim 1$ meV and $\sim 1.5$ meV for the ground-state and metastable solutions, respectively. There are also notable differences in the shape of potentials. For example, a flattened region appears for the metastable solutions. The minima in the outer regions are located at different distances from the center of the QPC. In both cases one finds, as to be expected, Friedel-like oscillation.

*Transmission and wave-function characteristics*. To explain the zero-bias anomaly in the conductance, Meir *et al.*[11] have recently proposed an Anderson model. Such a model requires that there are some kind of localized bound states associated with the QPC. For a wide and tall barrier these authors have argued that there are, in addition to the exponentially increasing transparency, narrow transmission resonances above the barrier. This would result from multiple reflections from the edges of the barrier, and are related to quasibound states, which can play the role of localized states in an Anderson model. This would be true for, let us say, a sharp rectangular barrier. In the present case, however, our simulations show that the barriers have soft features. In general, they are more like a gentle parabolic saddle-point potential, which does not display resonances from quasibound resonances.

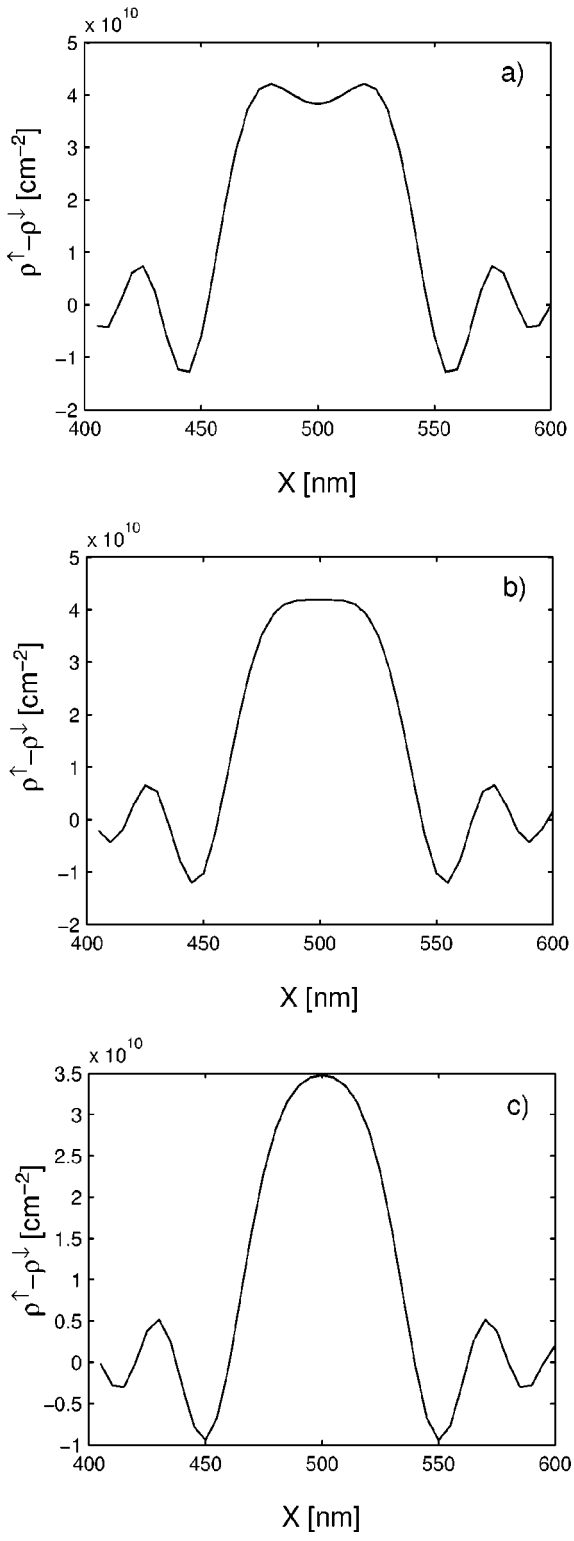


FIG. 5. Local spin polarization along the transport axis in the middle of wire for different split-gate voltages $V_{sg}=-0.720$ (a), $V_{sg}=-0.717$ (b), $V_{sg}=-0.714$ (c).

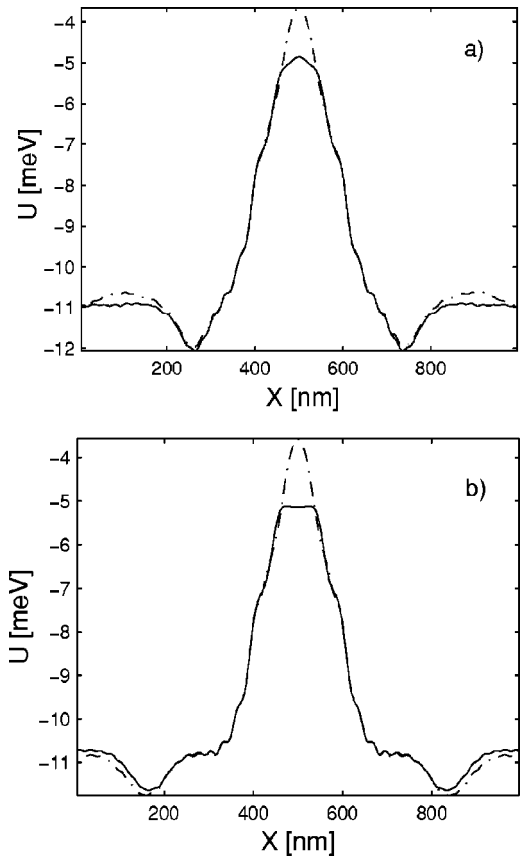


FIG. 6. Spin-polarized self-consistant total potentials for $\sigma=\uparrow$ (solid line) and $\sigma=\downarrow$ (dashed line) along transport axis in the middle of the device at $V_{sg}=-0.715$ V; (a) and (b) refer to the ground-state and the unstable solutions, respectively [solid and dashed curves in Fig. 3(b)]. (Although oversimplified, we may say that an incoming electron at the Fermi level $E_f=0$ is essentially divided into ''transverse'' and ''longitudinal motions.'' Thus the longitudinal motion is the one that determines the transmission. Therefore we have full transmission for up-spin in the graphs shown here, while it is strongly reduced for the opposite spin direction.

To clarify this issue we have calculated transmission as a function of energy for different open transmission channels. In order not to miss some potentially very narrow resonance peaks, we have varied the energy in minute steps. Results for the transmissions, which are shown in Fig. 7, refer to the self-consistent ground-state solution in Fig. 3(b). Irrespective of the energy resolution chosen we find that all the transmissions increase monotonously with energy. Hence, there are no traces of transmission peaks and oscillations. The same qualitative picture is found also for the self-consitent potentials corresponding to different split-gate voltages $V_{sg}$. We have also investigated the higher states in Fig. 3(b) in the same way. Also in this case the results are negative. *We thus conclude that there are no quasibound states or resonances, at least for the present realistic device parameters.*

Although the self-consistent calculations also do not show quasibound states, the individual scattering states show intriguing features in the QPC region. The self-consistent states displayed in Fig. 8 are typical. Evidently, there is an

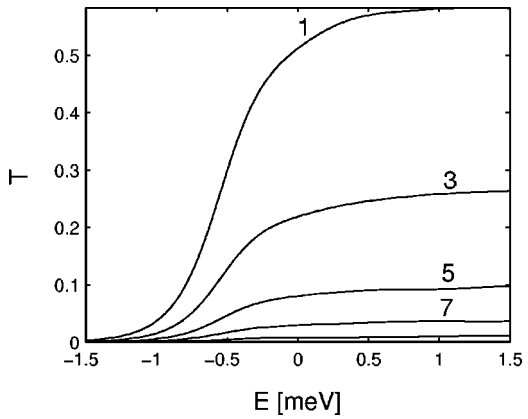


FIG. 7. Transmission through a QPC for electrons injected via different transfer modes and energy. The QPC potential is obtained from the self-consistent calculations for the split-gate voltage $V_{sg}=-0.715$ V. The results refer to the ground-state solution in Fig. 3(b). The labeling defines the different injection channels. For odd numbers the channel transmission vanishes because of symmetry.

accumulation of the individual transmitting states inside the QPC in spite of the overall reduction of total density. This feature is generic, it applies to all scattering states and must not be taken as an indication of quasibound states. Figure 9 shows a number of the scattering states in more detail for different spins and at two different voltages.

It is easy to understand why the accumulation within the QPC takes place. Each scattering state carries a current which must be same for all cross sections. In the wide reservoirs the local longitudinal wave number is high while the local amplitude may be low. In the QPC, on the other hand, the situation must be the reverse one if the total current is to be preserved. Thus the accumulation is easy to understand as a necessary consequence for current conservation. It is also found, however, for equilibrium situations such as a QPC connecting two quantum dots in which there is no current flow.[7]

## IV. SUMMARY

We have simulated the zero-temperature conductance in a realistic GaAs/AlGaAs split-gate QPC device using the spin-

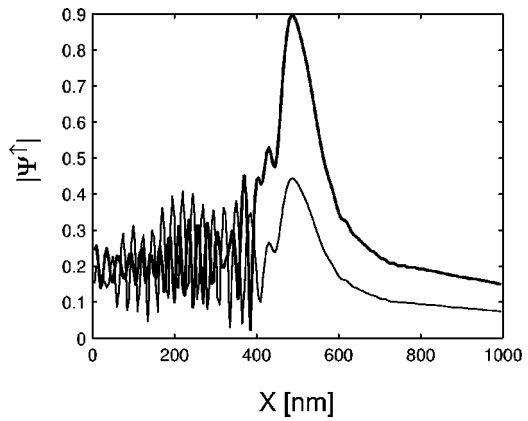


FIG. 8. Absolute values of two typical scattering states along the symmetry axis of the device. Electrons with $E=E_f$ are injected in the first (thick line) and third modes (thin line) at $V_{sg}=-0.715$.

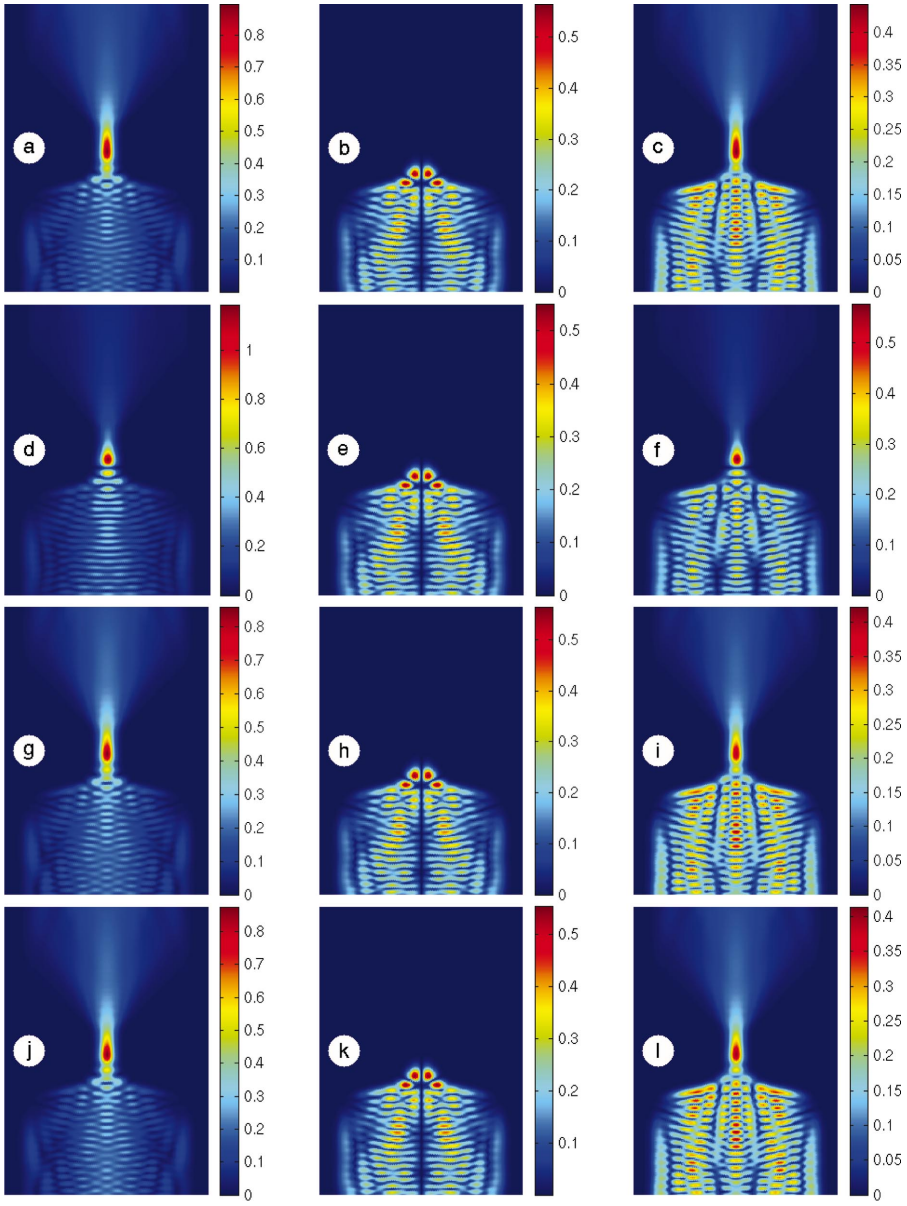


FIG. 9. (Color) Absolute value of scattering states with energy $E=E_f$. (a) $V_{sg}=-0.715$, $\sigma=\uparrow$, first mode. (b) $V_{sg}=-0.715$, $\sigma=\uparrow$, second mode. (c) $V_{sg}=-0.715$, $\sigma=\uparrow$, third mode. (d) $V_{sg}=-0.715$, $\sigma=\downarrow$, first mode. (e) $V_{sg}=-0.715$, $\sigma=\downarrow$, second mode. (f) $V_{sg}=-0.715$, $\sigma=\downarrow$, third mode. (g) $V_{sg}=-0.699$, $\sigma=\uparrow$, first mode. (h) $V_{sg}=-0.699$, $\sigma=\uparrow$, second mode. (i) $V_{sg}=-0.699$, $\sigma=\uparrow$, third mode. (j) $V_{sg}=-0.699$, $\sigma=\downarrow$, first mode. (k) $V_{sg}=-0.699$, $\sigma=\downarrow$, second mode. (l) $V_{sg}=-0.699$, $\sigma=\downarrow$, third mode.

relaxed Kohn-Sham equations. As in previous studies, we recover conduction anomalies associated with local magnetization that modifies the transmission barrier for the two spin directions in different ways. We have used two models: (a) with exchange only, and (b) with exchange and correlation potentials included. Both cases give rise to two anomalies although (a) overestimates the magnetization. It is, however, computationally relatively stable and we have therefore also been able to study higher subbands for the first time, to the best of our knowledge. In accordance with experiments, we recover smaller replicas in the second and third subbands.

In case (b) the introduction of correlation weakens the polarization, and as a consequence the conductance is increased towards normal conduction. The simulations were carried out with a variation of initial conditions for the iteration procedure. Making random choices of the initial potential, we have found that there are multisolutions in a range of voltages where an anomalous temperature dependence in the conductance is observed. We have suggested that measurements may be analyzed in these terms. As the temperature is raised the metastable states become thermally activated, and as a consequence the conductance decreases for a given voltage. We have also suggested that a similar mechanism may take place with increasing source-drain voltage $V_{sd}$. Further work should be performed along these lines including the effects of magnetic field. Unfortunately, the Kohn-Sham equations for finite temperatures are not readily available for the 2D systems discussed here.

We have also studied the nature of the scattering states because of the proposition of resonant or quasibound states.[11,12] For the realistic split-gate device studied we do not recover this kind of states. This negative result might be related to device geometry. In our case there are as much as 20 subbands in the source and drain regions, i.e., the regions are effectively two dimensional, while in Refs. 11 and 12 there are just two channels in the leads. Therefore, in the latter case the system is more like a long two-channel parabolic wire with a local constriction. The difference between

the two devices should make an interesting case for the experimentation of the role of geometry, electron densities, etc.

Finally, one should add a few words of caution about the Kohn-Sham equations. Here we make use of excited states, but to be strict, the LSDA is designed for ground-state properties. The form of correlation potential also raises questions. Although numerically small, we have noticed that the results are sensitive to this term. Different approximate algebraic expressions for $U_{cr}^{\sigma}(\mathbf{r})$ may therefore give different numbers, but supposedly not a qualitatively different scenario. This point should, of course, be tested in future work. In the simulations, we have allowed a collinear magnetism only. This was done for computational convenience but there is no principal reason for not extending the modeling to noncollinear situations as well. Such work is in progress.

*Note added in proof.* Recently P. S. Cornaglia and C. A. Balseiro have studied the magnetic nature of quantum point contacts and quasibound states.[21] G. Seelig and K. A. Matveev have drawn attention to electron-phonon scattering.[22]

## ACKNOWLEDGMENTS

This work has been supported by the Royal Swedish Academy of Sciences and The Swedish Natural Science Research Council NFR (now The Swedish Research Council VR). The computations were in part performed at the National Supercomputer Center at Linköping University.

[1] D.A. Wharam, T.J. Thornton, R. Newbury, M. Pepper, H. Ritchie, and G.A.C. Jones, J. Phys. C **21**, L209 (1988).
[2] B.J. van Wees, H. van Houten, C.W.J. Beenakker, J.G. Williamson, L.P. Kouwenhoven, D. van der Marel, and C.T. Foxton, Phys. Rev. Lett. **60**, 848 (1988).
[3] K.J. Thomas, J.T. Nicholls, M.Y. Simmons, M. Pepper, D.R. Mace, and D.A. Ritchie, Phys. Rev. Lett. **77**, 135 (1996).
[4] R. Fitzgerald, Phys. Today **55**(5), 21 (2002).
[5] K.-F. Berggren and M. Pepper, Phys. World **15(10)**, 37 (2002).
[6] J. R. Minkel, Phys. Rev. Focus **10**, 24 (2002).
[7] K.-F. Berggren and I.I. Yakimenko, Phys. Rev. B **66**, 085323 (2002).
[8] D.J. Reilly, T.M. Buehler, J.L. O'Brien, A.R. Hamilton, A.S. Dzurak, R.G. Clark, B.E. Kane, L.N. Pfeiffer, and K.W. West, Phys. Rev. Lett. **89**, 246801 (2002).
[9] P.E. Lindelof, Proc. SPIE **4415**, 77 (2001).
[10] S.M. Cronenwett, H.J. Lynch, D. Coldhaber-Gordon, L.P. Kouwenhoven, C.M. Marcus, K. Hirose, N.S. Wingreen, and V. Umansky, Phys. Rev. Lett. **88**, 226805 (2002).
[11] Y. Meir, K. Hirose, and N.S. Wingreen, Phys. Rev. Lett. **89**, 196802 (2002).
[12] K. Hirose, Y. Meir, and N.S. Wingreen, Phys. Rev. Lett. **90**, 026804 (2003).
[13] D. Schmeltzer, cond-mat/0211490 (unpublished).
[14] R.G. Parr and W. Yang, *Density-Functional Theory of Atoms and Molecules* (Oxford University Press, New York, 1989).
[15] J.H. Davies, Semicond. Sci. Technol. **3**, 995 (1988); J.H. Davies, I.A. Larkin, and E.V. Sukhorukov, J. Appl. Phys. **77**, 4504 (1995).
[16] B. Tanatar and D.M. Ceperley, Phys. Rev. B **39**, 5005 (1989).
[17] T. Ando, Phys. Rev. B **44**, 8017 (1991).
[18] C.-K. Wang and K.-F. Berggren, Phys. Rev. B **57**, 4552 (1998).
[19] K.J. Thomas, J.T. Nicholls, N.J. Appleyard, M.Y. Simmons, M. Pepper, D.R. Mace, W.R. Tribe, and D.A. Ritchie, Phys. Rev. B **58**, 4846 (1998).
[20] K.S. Pyshkin, C.J.B. Ford, R.H. Harrel, M. Pepper, E.H. Linfield, and D.A. Ritchie, Phys. Rev. B **62**, 15 842 (2000).
[21] P. S. Cornaglia and C. A. Balseiro, cond-mat/0304168 (unpublished).
[22] G. Seelig and K. A. Matveev, Phys. Rev. Lett. **90**, 176804 (2003).